arXiv:1610.02546v1 [cond-mat.mes-hall] 8 Oct 2016

Pure spin current and perfect valley filter by designed separation of the chiral states in two-dimensional honeycomb lattices

Da-Ping Liu,[1] Zhi-Ming Yu,[2,3,*] and Yu-Liang Liu[1,†]

[1] *Department of Physics, Renmin University of China, Beijing 100872, China*
[2] *Beijing Key Laboratory of Nanophotonics and Ultrafine Optoelectronic Systems, School of Physics, Beijing Institute of Technology, Beijing 100081, China*
[3] *Research Laboratory for Quantum Materials, Singapore University of Technology and Design, Singapore 487372, Singapore*

(Dated: October 11, 2016)

We propose a realization of pure spin currents and perfect valley filters based on a quantum anomalous Hall insulator, around which edge states with up-spin and down-spin circulate. By applying staggered sublattice potential on the strips along the edges of sample, the edge states with down spin can be pushed into the inner boundaries of the strips while the other edge states with up spin remain on the outer boundaries, resulting in spatially separated chiral states with perfect spin polarization. Moreover, a valley filter, which is immune to short-range and smooth long-range scatterers, can be engineered by additionally applying boundary potentials on the outmost lattices of the sample. We also find that the boundary potential can be used to control the size effect induced oscillation of the inner chiral states. The connection of the boundary potential to size effect is revealed.

PACS numbers: 73.43.-f, 72.25.-b, 73.63.-b, 71.70.Ej

I. INTRODUCTION

The extensive research on spintronics and valleytronics unveil that many binary degrees of freedom of electrons, e.g., spin and valley can be used to improve the efficiency of electronic devices[1–4]. Economic consideration makes designing electronic devices with both various degrees of freedom and low power consumption quite an attractive study area. Although various kinds of non-dissipative chiral (helical) modes have been theoretically proposed and experimentally realized[5–12], it is yet desirable to present an easy way to spatially separate all the chiral states to obtain currents with a pure degree polarization, such as pure spin (valley) current[13–15], as well as to independently manipulate them. Particularly, the chiral states pushed away from the boundaries will be immune to the boundary perturbations[16], such as the dangling bonds and boundary defects, which generally are obstacles for the application of the topological edge states.

When a system hosts two or more spatially separated chiral states, the influence of finite size effect on the chiral states may be significant[17–19]. The size effect can induce a undesired gap if the two chiral states with same momentum have overlap in the real space. Generally, one can eliminate the gap by shifting the momentum of the two chiral states[17]. However, the influence of size effect on the spatial distribution of the chiral states would persist even if the spectrum is gapless.

In this paper, we propose a scheme for spatially separating all the edge states of a quantum anomalous Hall (QAH) insulator with Chern number $|\mathcal{C}| = 2$ based on two-dimensional honeycomb lattices to realize pure spin currents. The QAH effect can be introduced into honeycomb lattices if one considers the Haldane term, which was artificially proposed at first[20]. But later, it turns out that the Haldane term can be realized in laser-driven systems[8,21,22], where the low-energy electrons submit to the Floquet theory[22–26]. Usually, the honeycomb lattices also may possess sizeable intrinsic spin-orbit coupling (SOC)[27–29], thus in such case the appearance of QAH effect requires that the Haldane term should dominate the SOC.

In the presence of Haldane term and SOC, a QAH insulator with $|\mathcal{C}| = 2$ can be generated. At each edge of the QAH sample, the two unipropagating edge states are of up-spin and down-spin respectively and thus, the edge current is spin unpolarized. By applying staggered sublattice potential to narrow strips along the two edges, one pair of the edge states with down-spin can be pushed to the inner boundaries of the potential regions, while the other with up-spin will be still at the outer boundaries. With the help of local terminals, the spatially separated pure spin currents can be independently extracted out. Moreover, by additionally applying potentials on the outmost lattices of the sample, all the chiral states will reside around the valley points and the velocity of them can be valley dependent[30], giving rise to a perfect valley filter, as the counterpropagating chiral states are well separated in both real and momentum space. Also, the spin and valley index of the inner chiral states can be switched by changing the sign of Haldane term (e.g. switching the polarized direction of the circularly polarized laser) and the direction of the staggered potential. The finite size effect will induce an oscillation on the spatial distribution of the inner chiral states. Interestingly, we find that a local rather than global manipulation tuning the boundary potential can effectively control the size effect induced oscillation.

Our paper is organized as follows. In Sec. II, we introduce a model Hamiltonian of honeycomb lattices with intrinsic SOC and Haldane term under a spatial depen-

dent potential. Section III describes the spatial separation of chiral edge states and the realization of perfect valley filter. We investigate the size effect induced oscillation of the inner chiral states in Sec. IV. Finally, we present some discussions and conclusions in Sec. V.

II. MODEL HAMILTONIAN

We start from a tight-binding (TB) Hamiltonian defined on a two-dimensional honeycomb lattice $\mathcal{H} = \mathcal{H}_0 + \mathcal{H}_1$ with

$$\mathcal{H}_0 = -t\sum_{\langle i,j\rangle\alpha} c^\dagger_{i\alpha}c_{j\alpha} + i\frac{\lambda}{3\sqrt{3}}\sum_{\langle\langle i,j\rangle\rangle\alpha\beta} v_{ij}c^\dagger_{i\alpha}\tau^z_{\alpha\beta}c_{j\beta} + i\frac{\lambda_\omega}{3\sqrt{3}}\sum_{\langle\langle i,j\rangle\rangle\alpha} v_{ij}c^\dagger_{i\alpha}c_{j\alpha}, \quad (1)$$

where τ^z is z-component Pauli matrix. t is the nearest-neighbor hopping. λ and λ_ω represent the strength of intrinsic SOC and Haldane term respectively. The Haldane term can be induced by an off-resonance coherent and circularly polarized laser beam. $v_{ij} = +(-)$ if the hopping from site j to site i is anticlockwise (clockwise) with respect to the positive z axis[31]. And

$$\mathcal{H}_1 = \textstyle\sum_i \mu_i\Delta c^\dagger_{i\alpha}c_{i\alpha}, \quad (2)$$

represents a staggered sublattice potential with $\mu_i = +(-)$ for the A (B) site, which may be induced by substrate[32] or by simply applying an external electric field if the system is buckled[33,34].

To gain a transparent understanding of the topological properties of $\mathcal{H}$ and the following discussions of spatial separation of the chiral edge modes, we write down the low-energy Hamiltonian around the valley points,

$$H = v_{\rm F}\left(\eta k_x\sigma_x + k_y\sigma_y\right) + \left[\Delta - \eta\left(\lambda s_z + \lambda_\omega\right)\right]\sigma_z, \quad (3)$$

where $v_{\rm F} = \sqrt{3}a_0t/2$ is the Fermi velocity with a_0 the lattice constant. Pauli matrices $\boldsymbol{\sigma}$ act on the sublattice pseudospin, $\eta = +$ $(-)$ denotes the valley index K (K'), and $s_z = +$ $(-)$ represents up (down) spin. According to Hamiltonian (3), the valley-contrasting topological charge is[9,30,35]

$$\mathcal{C}_{s_z,\eta} = \frac{\eta}{2}\times{\rm sgn}[\Delta - \eta(\lambda s_z + \lambda_\omega)]. \quad (4)$$

In the absence of potential $\Delta = 0$, the system is a QAH (quantum spin Hall) insulator if $|\lambda_\omega| > |\lambda|$ ($|\lambda_\omega| < |\lambda|$). Since we are interested in a QAH sample here, without loss of generality, we let $\lambda_\omega > \lambda > 0$, and the following discussions can be directly extended to the case of $\lambda_\omega < 0$ and $|\lambda_\omega| > |\lambda|$. If $|\Delta| < \lambda_\omega - \lambda$, the topological properties of system are the same with that of $\Delta = 0$. On the other hand, if $|\Delta| > \lambda_\omega + \lambda$, then $\mathcal{C}_{s_z,\eta}(\Delta) = \frac{\eta}{2}{\rm sgn}[\Delta]$ is only determined by the sign of Δ. The interesting case is that when $|\Delta| \in (\lambda_\omega - \lambda, \lambda_\omega + \lambda)$, $\mathcal{C}_{+,\eta}(\Delta) = \frac{1}{2}$ and $\mathcal{C}_{-,\eta}(\Delta) = \frac{\eta}{2}{\rm sgn}[\Delta]$. In this case, band structure of electron with $s_z = 1$ is still topology nontrivial while that of electron with $s_z = -1$ is topology trivial, as the total Chern number of up (down) spin is $\sum_\eta \mathcal{C}_{+,\eta} = 1$ ($\sum_\eta \mathcal{C}_{-,\eta} = 0$). Thus, the potential $|\Delta| \in (\lambda_\omega - \lambda, \lambda_\omega + \lambda)$ only changes the topological properties of down-spin.

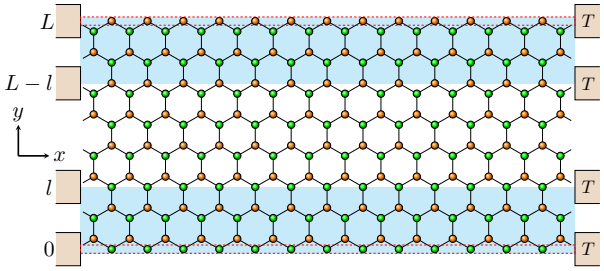

FIG. 1. (Color online) Schematic of a QAH sample with two long strips geometry. The two sublattices A and B are denoted by olive and red balls respectively. And the profile of the y-dependent staggered sublattice potential is shown by the color in the nanoribbon. The local terminal (T) can extract the spin perfectly polarized current out.

Based on the above discussions, we consider a QAH sample with strips applied on different potential, as shown in Fig. 1. The potential Δ is chosen to be nonzero in region I ($0 < y < l$) and region III ($L - l < y < L$), and vanishing in region II ($l < y < L - l$). One can find that if $|\Delta_{\rm I(III)}| \in (\lambda_\omega - \lambda, \lambda_\omega + \lambda)$, then for the electrons with $s_z = -1$, region II will be topologically distinct from the others, while for the electrons with $s_z = 1$, the three regions are still topologically equal. According to the bulk-boundary correspondence[36], there would be chiral modes with $s_z = -1$ appear at the boundaries of region II. While the pair of edge states with $s_z = 1$ would be still at the outer boundaries. Moveover, from the index theorem[35–37], one has $v^{\rm I(III)}_{s_z,\eta} = \mathcal{C}_{s_z,\eta}(\Delta_{\rm I(III)}) - \mathcal{C}_{s_z,\eta}(\Delta_{\rm II})$, where $v^{\rm I(III)}_{s_z,\eta}$ is the number of chiral modes with index s_z and η located at the interface of region I (III) and region II. In the case of $|\Delta_{\rm I(III)}| \in (\lambda_\omega - \lambda, \lambda_\omega + \lambda)$, one has

$$v^{\rm I(III)}_{+,\eta} = 0;\ v^{\rm I(III)}_{-,\eta} = \frac{1}{2}\left[\eta\times{\rm sgn}\left(\Delta_{\rm I(III)}\right) + 1\right], \quad (5)$$

indicating that the inner chiral states must be of $s_z = -1$ and of $\eta = {\rm sgn}[\Delta_{\rm I(III)}]$. And the valley index of the inner chiral state can be switched by changing the sign of $\Delta_{\rm I(III)}$.

III. PURE SPIN CURRENT AND PERFECT VALLEY FILTER

In the present model, spin is always a good quantum number. For the pristine QAH sample ($\Delta_{\rm I} = \Delta_{\rm III} = 0$), the edge currents propagating along the edges of sample are spin unpolarized, as they simultaneously contain up-spin and down-spin. By applying suitable potential $|\Delta_{\rm I(III)}| \in (\lambda_\omega - \lambda, \lambda_\omega + \lambda)$, four spin perfect polarized

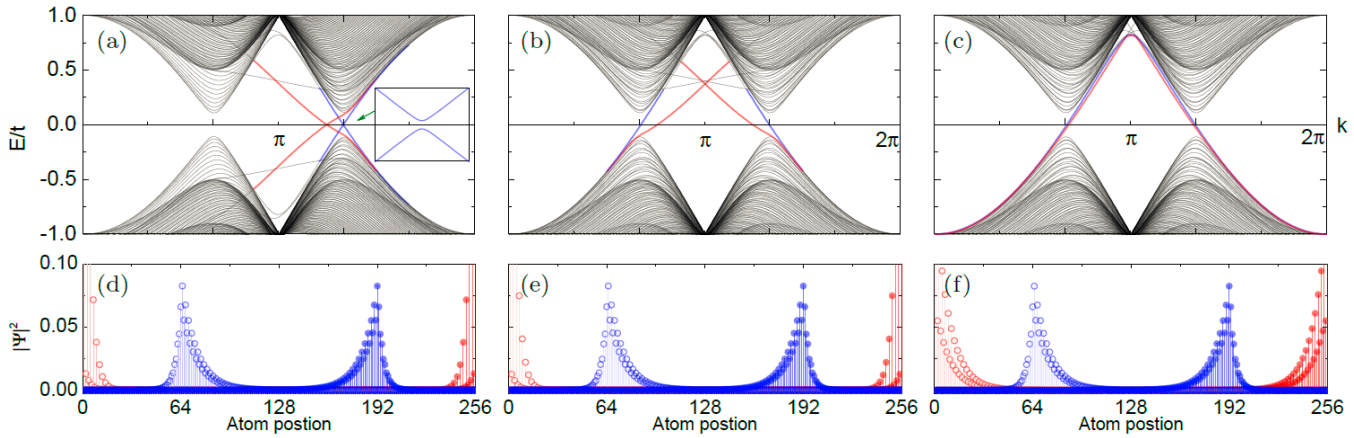

FIG. 2. (Color online) Band structures of the QAH nanoribbon for (a) $\Delta_{\rm I} = \Delta_{\rm III} = 0.4\,t$, (b) $\Delta_{\rm I} = -\Delta_{\rm III} = 0.4\,t$ and (c) $\Delta_{\rm I} = -\Delta_{\rm III} = 0.4\,t$ with boundary potential $\Delta'_{\rm I} = -\Delta'_{\rm III} = t$. (d-f) Corresponding spatial distribution of the four chiral states near Fermi energy. The chiral states with up-spin (down-spin) are denoted by red (blue) lines. And the solid (hollow) circles correspond to right- (left-)propagating chiral states. In the figures, we choose $\lambda = 0.2\,t$, $\lambda_\omega = 0.3\,t$, $L = 256$ atoms, and $l = 64$ atoms.

currents are generated propagating along the four interfaces $y = 0$, l, $L - l$, and L respectively [Fig. 2(a) and 2(b)]. With the help of local terminals (schematically shown in Fig. 1), pure spin currents can be extracted out whenever the distance between the four interfaces (e.g. l and $L - 2l$) are much larger than the spatial broadening of the chiral states, which generally can be satisfied by choosing suitable parameters as shown in Fig. 2. Also, the valley index of the inner chiral states can be independently manipulated by switching the sign of $\Delta_{\rm I}$ or $\Delta_{\rm III}$ [Eq. (5)]. Hence the two inner chiral states can have same ($\Delta_{\rm I}\Delta_{\rm III} > 0$) or different ($\Delta_{\rm I}\Delta_{\rm III} < 0$) valley index. Particularly, when $\Delta_{\rm I}\Delta_{\rm III} < 0$, the two inner chiral states locate at different valley and would be always gapless regardless of width of region II [Fig. 2(b)]. Generally, the applied electric field and substrate can induce a weak Rashba SOC[31], which couples different spin modes[38]. However, the pure spin currents proposed here are robust against a weak Rashba SOC, as all the chiral (spin) modes are spatially separated.

In the present model, a perfect valley filter also can be engineered by additionally applying boundary potentials $\Delta'_{\rm I(III)}$ on the outermost sites of sample (marked by the red frame in Fig. 1). Let us start from Fig. 2(b) where $\Delta_{\rm I}\Delta_{\rm III} < 0$. The outer edge states (denoted as red lines), which do not have well defined valley index in such case, mainly concentrate on the boundaries of sample as shown in Fig. 2(e). By tuning the boundary potentials $\Delta'_{\rm I(III)}$, the two outer edge band dispersion can bend upward and gradually merge into the bulk conduction band[30]. At the same time, the zero mode of the outer edge states would reside around the corresponding valley points [Fig. 2(c)]. Consequently, all the four chiral states possess well-defined valley index and the velocity of them is valley dependent. Since the counter-propagating chiral states are well separated in both real and momentum space, the valley filter and pure spin currents proposed here would be immune to short-range scatterers, as well as the long-range scatterers that are smooth at the atomic scale.

IV. SIZE EFFECT

In this section, we study the finite size effect on the chiral modes. Without resorting to the detailed analysis, one can obtain several key features of the size effect: (1) Size effect is induced by the interfaces of system, including the boundaries and the inner interfaces. The boundaries of sample would have stronger limit effect than that of the inner interface, as the electrons can pass through the inner interfaces but are forbidden to be out of sample. (2) If the chiral modes intersect in the momentum space, the size effect can produce a width dependent gap [Fig. 2(a)]. (3) The wavefunction of the chiral mode is determined by the boundary conditions. Hence the inner chiral states in the present model would have distinct wavefunction compared with the chiral modes in a perfect domain wall and the edge states located at the boundary of sample. The size effect on the spectrum of chiral modes have been studied in previous wroks[17,18]. In this paper, we focus on the influence of size effect on the wavefunction of the inner chiral modes. We find that the inner chiral mode would possess peculiar oscillated wavefunction induced by the size effect and interestingly, this oscillation can be controlled by a local manipulation tuning the boundary potential.

The inner chiral mode is reminiscent of the chiral mode in a domain wall respecting Jackiw-Rebbi solution[39], of which the general form is[10]:

$$\Psi_D(x,y) = \begin{pmatrix} \phi_A(y) \\ \phi_B(y) \end{pmatrix} = \frac{1}{\mathcal{N}} \begin{pmatrix} 1 \\ -i \end{pmatrix} e^{ik_x x + (y-l)\kappa(y)}, \quad (6)$$

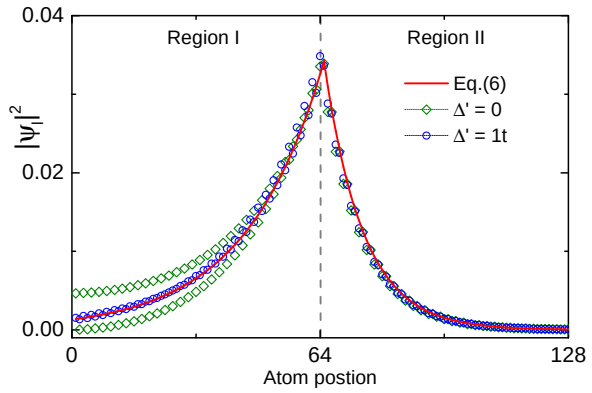

FIG. 3. (Color online)The influence of boundary potential Δ' on the size effect induced oscillation. Spatial distribution of the inner chiral state $|\Psi_l(x,y)|^2$ at K valley point for different Δ' are plotted. The red solid lines are from Eq. (6) and the hollow circles are solutions from the TB model with different Δ'. In the figure, we choose $\lambda = 0.2\,t$, $\lambda_\omega = 0.3\,t$, $\Delta_{\rm I} = 0.15\,t$, $\Delta_{\rm III} = -0.15\,t$, $l = 64$ atoms and the ribbon width $L = 256$ atoms.

where the location of domain wall is chosen to be $y = l$, $\mathcal{N}$ is the normalization constant, and $\phi_{A(B)}$ is the wavefunction of A (B) sublattice. When ribbon width is infinite that $L \gg l \gg 0$, there is no size effect and the inner chiral state $\Psi_l(x,y)$ (located at $y = l$) would be the same as $\Psi_D(x,y)$, with $\kappa(y) = \kappa_{\rm I} \equiv (\Delta_{\rm I} + \lambda - \lambda_\omega)/v_{\rm F}$ for $y < l$ and $\kappa(y) = \kappa_{\rm II} \equiv (\lambda - \lambda_\omega)/v_{\rm F}$ for $y > l$ (here we choose $\Delta_{\rm I} > 0$, and $\Delta_{\rm I}\Delta_{\rm III} < 0$). When L is finite but $\kappa_{\rm I} l \gg 1$, $\Psi_l(x,y)$ would be still almost the same as $\Psi_D(x,y)$. On the other hand, when $\kappa_{\rm I} l \simeq 1$, $\Psi_l(x,y)$ would deviate from $\Psi_D(x,y)$, corresponding to the presence of a finite size effect. In Fig. 3, we plot the spatial distribution of the inner chiral state $|\Psi_l(y)|^2$ with $k_y = 2\pi/3$ (K valley point) and the potential $\Delta_{\rm I}$ chosen to satisfy $\kappa_{\rm I} l \simeq 1$. In region I, $|\Psi_l(y)|^2$ (olive rhombus) presents an oscillation around $|\Psi_D(y)|^2$ (red line). One can understand this oscillation by the geometry of the zigzag nanoribbon. For a zigzag nanoribbon, $\phi_A(y)$ and $\phi_B(y)$ obey symmetric quadratic differential equation but different boundary conditions[40] that $\phi_B(0) = 0$ while $\phi_A(0)$ is finite except in the limit of no size effect that $\kappa_{\rm I} l \gg 1$, thus the behavior of $\phi_A(y)$ and $\phi_B(y)$ are very different when $\kappa_{\rm I} l \simeq 1$, leading to the oscillation.

The oscillation amplitude of $|\Psi_l(y)|^2$ generally can be controlled by changing l and $\kappa_{\rm I}$. However, we find that a local manipulation tuning the boundary potential also can be used to control the size effect induced oscillation. With finite l, one does not have $|\phi_A(0)| = |\phi_B(0)|$ in a zigzag nanoribbon, however $|\phi_A(0^+)| = |\phi_B(0^+)|$ is possible, in such case the behavior of $|\phi_A(y)|$ and $|\phi_B(y)|$ in region I will be identical except $y = 0$ and thus the size effect induced oscillation is eliminated. To realize above situation, one needs to introduce a delta function $[\delta(0)\sigma_z]$ to make $\phi_{A(B)}(y)$ to be discontinuous at $y = 0$. The delta function $\delta(0)\sigma_z$ in low-energy continuum model corresponds to an abrupt change of potential at boundary $y = 0$ in a TB lattice model, which is nothing but tuning the boundary potential Δ'. The influence of Δ' on the oscillation is shown in Fig. 3 too. By increasing Δ' from zero, $|\phi_B(0^+)|$ will increase from zero, which inevitably leads to the decrease of $|\phi_A(0^+)|$ as the total wavefunction $\Psi_l(y)$ is normalized. When Δ' approaches a critical value Δ'_c, one would have $|\phi_B(0^+)| = |\phi_A(0^+)|$ and the oscillation is eliminated. If one keeps increasing Δ', $|\phi_B(0^+)|$ will be larger than $|\phi_A(0^+)|$ and the oscillation will reappear.

The connection of the boundary potential to size effect induced oscillation can be quantitatively understood within a Dirac equation. Consider the TB Hamiltonian with boundary potential Δ',

$$\mathcal{H}' = \mathcal{H} + \Delta' c^\dagger_{y=0,A} c_{y=0,A}, \tag{7}$$

with $\mathcal{H} = \mathcal{H}_0 + \mathcal{H}_1$. The wavefunction of the chiral state $\Psi_l(y)$ can be obtained by the corresponding Dirac equation[40–42] defined around K valley ($\Delta_{\rm I} > 0$)

$$H' = v_F\left(k_x\sigma_x - i\partial_y\sigma_y\right) + \left(\bar{\Delta}(y) + \bar{y}\Delta'\delta_{y=0}\right)\sigma_z, \tag{8}$$

where $\bar{\Delta}(y) = \Delta_{\rm I} + \lambda - \lambda_\omega$ ($= \lambda - \lambda_\omega$) in region $y < l$ ($y > l$) and $\bar{y} = \sqrt{3}a_0/2$ is the average distance of site A (or B) along the y direction. Integrating Eq. (8) around $y = 0$ and considering that $\phi_B(0) = 0$, one has

$$\Delta'\bar{y}\phi_A(0) = \Delta'\bar{y}\phi_A(0^+) = iv_F\phi_B(0^+), \tag{9}$$

which directly show that when $\Delta' = t$, $|\phi_A(0^+)| = |\phi_B(0^+)|$. From Fig. 2, one also observes that the energy of the inner chiral states located at valley point is close to zero $\varepsilon_l(k_y = 2\pi/3) \approx 0$. In the case of $\bar{\Delta}(y < l) \gg \varepsilon_l(2\pi/3)$, one can approximately let $\varepsilon_l(2\pi/3) = 0$ and then has

$$\Psi_l(x,y) \approx \frac{1}{\mathcal{N}_l}\begin{pmatrix} e^{y\kappa_{\rm I}} + \gamma e^{-y\kappa_{\rm I}} \\ -i\left(e^{y\kappa_{\rm I}} - \gamma e^{-y\kappa_{\rm I}}\right)\end{pmatrix}, \tag{10}$$

for $0 < y < l$, where $\mathcal{N}_l$ is the normalization constant and

$$\gamma = \frac{v_{\rm F} - \bar{y}\Delta'}{v_{\rm F} + \bar{y}\Delta'} = \frac{t - \Delta'}{t + \Delta'}. \tag{11}$$

For $y > l$, $\Psi_l(x,y)$ would have the same expression with $\Psi_D(x,y)$ up to a normalization constant whenever $L - 2l \gg v_F/\bar{\Delta}(y > l)$. From Eq. (10), one knows that when $\Delta' = t$, $\gamma = 0$ and $\Psi_l(x,y)$ will be identical with $\Psi_D(x,y)$ in both regions $0 < y < l$ and $y > l$ (up to a normalization constant), and thus the size effect induced oscillation would be approximately eliminated, as shown in Fig. 3. When $\Delta' = t$, $\Psi_l(x,y)$ has a rather simple expression and then the spatial distribution of the inner chiral modes can be directly obtained, which is helpful to the precise manipulation of these modes.

V. DISCUSSION AND CONCLUSION

We have proposed a model to realize pure spin current and perfect valley filter by spatially separating all the chiral modes of a QAH sample. Also we have presented a local control of the finite size effect induced oscillation of the inner chiral states.

Many of the already known two-dimensional honeycomb lattices, especially the buckled materials, may be used to realize the present proposals. First, the staggered sublattice potential can be easily induced and tuned by a perpendicular electric field in buckled systems. Second, buckled systems generally possess sizeable intrinsic SOC[28]. Third, the strength of Haldane term can be tuned by changing the intensity and frequency of the circularly polarized laser beam and the situation of $\lambda_\omega > \lambda$ may be satisfied[8,43]. Thus, silicene, germanene and stanene are suitable candidates[34], especially that silicene field-effect transistors have been recently fabricated at room temperature[44] and germanene has been successfully synthesized on a band gap material[45]. Notice that to realize the present proposal in a highly integrated microelectronic device is a challenging task, but our investigation undoubtedly provides an opportunity to generate the pure spin currents and perfect valley filter.

Overall, our proposals of generating pure spin currents and designing perfect valley filter may be realized in many honeycomb lattices. And the ease of electric field control of low-dimensional buckled materials would give rise to a wide application scope of the present proposal.

ACKNOWLEDGMENTS

The authors acknowledge discussions with Shengyuan A. Yang and Yugui Yao. This work is supported by the Fundamental Research Funds for the Central Universities, the Research Funds of Renmin University of China (14XNLQ03), and the National Basic Research Program of China (Grant No. 2012CB921704).

* zmyu@bit.edu.cn
† ylliu@ruc.edu.cn

[1] R. Hanson, L. P. Kouwenhoven, J. R. Petta, S. Tarucha, and L. M. K. Vandersypen, *Spins in few-electron quantum dots*, Rev. Mod. Phys. **79**, 1217 (2007).
[2] A. Rycerz, J. Tworzydło, and C. W. J. Beenakker, *Valley filter and valley valve in graphene*, Nat. Phys. **3**, 172 (2007).
[3] D. Xiao, W. Yao, and Q. Niu, *Valley-contrasting physics in graphene: magnetic moment and topological transport*, Phys. Rev. Lett. **99**, 236809 (2007).
[4] D. Xiao, G.-B. Liu, W. X. Feng, X. D. Xu, and W. Yao, *Coupled spin and valley physics in monolayers of MoS_2 and other group-VI dichalcogenides*, Phys. Rev. Lett. **108**, 196802 (2012).
[5] Z. Qiao, W. Tse, H. Jiang, Y. Yao, and Q. Niu, *Two-Dimensional Topological Insulator State and Topological Phase Transition in Bilayer Graphene*, Phys. Rev. Lett. **107**, 256801 (2011).
[6] F. Zhang, J. Jung, G. A. Fiete, Q. Niu, and A. H. MacDonald, *Spontaneous Quantum Hall States in Chirally Stacked Few-Layer Graphene System*, Phys. Rev. Lett. **106**, 156801 (2011).
[7] Di Xiao, W. Zhu, Y. Ran, N. Nagaosa, and S. Okamoto, *Interface engineering of quantum Hall effects in digital transition metal oxide heterostructures*, Nat. Comm. **2**, 596 (2011).
[8] M. Ezawa, *Photoinduced Topological Phase Transition and a Single Dirac-Cone State in Silicene*, Phys. Rev. Lett. **110**, 026603 (2013).
[9] H. Pan, X. Li, F. Zhang, and S. A. Yang, *Perfect valley filter in a topological domain wall*, Phys. Rev. B **92**, 041404 (2015).
[10] H. Pan, X. Li, H. Jiang, Y. Yao, and S. A. Yang, *Valley-polarized quantum anomalous Hall phase and disorder-induced valley-filtered chiral edge channels*, Phys. Rev. B **91**, 045404 (2015).
[11] S. Rachel and M. Ezawa, *Giant magnetoresistance and perfect spin filter in silicene, germanene, and stanene*, Phys. Rev. B **89**, 195303(2014).
[12] L. Ju et al., *Topological valley transport at bilayer graphene domain walls*, Nature (London) **520**, 650 (2015).
[13] Q.-D. Jiang, H. Jiang, H. Liu, Q.-F. Sun, and X. C. Xie, *Topological Imbert-Fedorov Shift in Weyl Semimetals*, Phys. Rev. Lett. **115**, 156602 (2015).
[14] S. A. Yang, H. Pan, and F. Zhang, *Chirality-Dependent Hall Effect in Weyl Semimetals*, Phys. Rev. Lett. **115**, 156603 (2015).
[15] H. Li, L. Sheng, R. Shen, L. B. Shao, B. Wang, D. N. Sheng, and D.Y. Xing, *Stabilization of the Quantum Spin Hall Effect by Designed Removal of Time-Reversal Symmetry of Edge States*, Phys. Rev. Lett. **110**, 266802 (2013).
[16] M. Wang, L. Liu, C.-C. Liu, and Y. Yao, *van der Waals heterostructures of germanene, stanene, and silicene with hexagonal boron nitride and their topological domain walls*, Phys. Rev. B **93**, 155412 (2016).
[17] B. Zhou, H. Lu, R. Chu, S. Shen, and Q. Niu, *Finite Size Effects on Helical Edge States in a Quantum Spin-Hall System*, Phys. Rev. Lett. **101**, 246807 (2008).
[18] M. Ezawa and N. Nagaosa, *Interference of topologically protected edge states in silicene nanoribbons*, Phys. Rev. B **88**, 121401 (2013).
[19] H.-H. Fu, J.-T. Lu, and J.-H. Gao, *Finite-size effects in the quantum anomalous Hall system*, Phys. Rev. B **89**, 205431 (2014).
[20] F. D. M. Haldane, *Model for a Quantum Hall Effect without Landau Levels: Condensed-Matter Realization of the "Parity Anomaly"*, Phys. Rev. Lett. **61**, 2015 (1988).
[21] A. Scholz, A. López, and J. Schliemann, *Interplay between spin-orbit interactions and a time-dependent electromagnetic field in monolayer graphene*, Phys. Rev. B **88**, 045118 (2013).

[22] T. Kitagawa, T. Oka, A. Brataas, L. Fu, and E. Demler, *Transport properties of nonequilibrium systems under the application of light: Photoinduced quantum Hall insulators without Landau levels*, Phys. Rev. B **84**, 235108 (2011).

[23] J. Cayssol, B. Dóra, F. Simon, and R. Moessner, *Floquet topological insulators*, Phys. Status Solidi RRL **7**, 101 (2013).

[24] A. López, A. Scholz, B. Santos, and J. Schliemann, *Photoinduced pseudospin effects in silicene beyond the off-resonant condition*, Phys. Rev. B **91**, 125105 (2015).

[25] Y. H. Wang, H. Steinberg, P. Jarillo-Herrero, and N. Gedik, *Observation of Floquet-Bloch States on the Surface of a Topological Insulator*, Science **342**, 453 (2013).

[26] M. C. Rechtsman, J. M. Zeuner, Y. Plotnik, Y. Lumer, D. Podolsky, F. Dreisow, S. Nolte, M. Segev, and A. Szameit, *Photonic Floquet topological insulators*, Nature (London) **496**, 196 (2013).

[27] J. Zhao, H. Liu, Z. M. Yu , R. Quhe, S. Zhou, Y. Wang, C. C. Liu, H. Zhong, N. Han, J. Lu, Y. Yao, and K. Wu, *Rise of silicene: A competitive 2D material*, Prog. in Mater. Sci. **83**, 24 (2016)

[28] C.-C. Liu, W. Feng, and Y. Yao, *Quantum Spin Hall Effect in Silicene and Two-Dimensional Germanium*, Phys. Rev. Lett. **107**, 076802 (2011).

[29] Z. Song, C.-C. Liu, J. Yang, J. Han, M. Ye, B. Fu, Y. Yang, Q. Niu, J. Lu, and Y. Yao, *Quantum spin Hall insulators and quantum valley Hall insulators of BiX/SbX (X=H, F, Cl and Br) monolayers with a record bulk band gap*, NPG Asia Mater. **6**, 147 (2014).

[30] W. Yao, S. A. Yang, and Q. Niu, *Edge States in Graphene: From Gapped Flat-Band to Gapless Chiral Modes*, Phys. Rev. Lett. **102**, 096801 (2009).

[31] C. L. Kane and E. J. Mele, *Quantum Spin Hall Effect in Graphene*, Phys. Rev. Lett. **95**, 226801 (2005).

[32] S. Y. Zhou, G.-H. Gweon, A. V. Fedorov, P. N. First, W. A. de Heer, D.-H. Lee, F. Guinea, A. H. Castro Neto, and A. Lanzara, *Substrate-induced bandgap opening in epitaxial graphene*, Nat. Mater. **6**, 770 (2007).

[33] Z. M. Yu, H. Pan, and Y.G. Yao, *Electric field controlled spin- and valley-polarized edge states in silicene with extrinsic Rashba effect*, Phys. Rev. B. **92**, 155419 (2015).

[34] C.-C. Liu, H. Jiang, and Y. Yao, *Low-energy effective Hamiltonian involving spin-orbit coupling in silicene and two-dimensional germanium and tin*, Phys. Rev. B **84**, 195430 (2011).

[35] I. Martin, Y. M. Blanter, and A. F. Morpurgo, *Topological Confinement in Bilayer Graphene*, Phys. Rev. Lett. **100**, 036804 (2008).

[36] G. E. Volovik, The Universe in a Helium Droplet (Oxford University Press, New York, 2003).

[37] G. W. Semenoff, V. Semenoff, and F. Zhou, *Domain Walls in Gapped Graphene*, Phys. Rev. Lett. **101**, 087204 (2008).

[38] K. Sengupta, R. Roy, and M. Maiti, it Spin Hall effect in triplet chiral superconductors and graphene, Phys. Rev. B. **74**, 094505 (2006).

[39] R. Jackiw and C. Rebbi, *Solitons with fermion number 1/2*, Phys. Rev. D **13**, 3398 (1976).

[40] L. Brey and H. A. Fertig, *Electronic states of graphene nanoribbons studied with the Dirac equation*, Phys. Rev. B **73**, 235411 (2006).

[41] S K Wang, J Wang and K S Chan, *Multiple topological interface states in silicene*, New Jour. Phys. **16**, 045015 (2014).

[42] K. Nakada, M. Fujita, G. Dresselhaus and M. S. Dresselhaus, *Edge state in graphene ribbons: Nanometer size effect and edge shape dependence*, Phys. Rev. B **54**, 17954 (1996).

[43] J. P. Dahlhaus, B. M. Fregoso, and J. E. Moore, *Magnetization Signatures of Light-Induced Quantum Hall Edge States*, Phys. Rev. Lett. **114**, 246802 (2015).

[44] L. Tao, E. Cinquanta, D. Chiappe, C. Grazianetti, M. Fanciulli, M. Dubey, A. Molle, and D. Akinwande, *Silicene field-effect transistors operating at room temperature*, Nat. Nanotechnol. **10**, 227 (2015).

[45] L. Zhang, P. Bampoulis, A. N. Rudenko, Q. Yao, A. van Houselt, B. Poelsema, M. I. Katsnelson, and H. J.W. Zandvliet, *Structural and Electronic Properties of Germanene on MoS_2*, Phys. Rev. Lett. **116**, 256804 (2016).